International Journal of Thermal Sciences 89 (2015) 43–57

Contents lists available at ScienceDirect

International Journal of Thermal Sciences

journal homepage: www.elsevier.com/locate/ijts

Comparison of thermal scaling properties between turbulent pipe and channel flows via DNS

S. Saha [a, *], J.C. Klewicki [a, b], A.S.H. Ooi [a], H.M. Blackburn [c]

[a] Department of Mechanical Engineering, University of Melbourne, Melbourne, VIC 3010, Australia
[b] Department of Mechanical Engineering, University of New Hampshire, Durham, NH 03824, USA
[c] Department of Mechanical and Aerospace Engineering, Monash University, VIC 3800, Australia

ARTICLE INFO

Article history:
Received 8 May 2014
Received in revised form
12 October 2014
Accepted 13 October 2014
Available online

Keywords:
Turbulent flow
Heat transfer
Channel
Pipe
Scaling

ABSTRACT

A systematic comparison of thermal scaling properties of pipe and channel flows is presented. DNS data are used to compute thermal statistics for friction Reynolds numbers of 180 and 395 and Prandtl numbers ranging between 0.025 and 7. A distinct four layer regime for the thermal field is clearly identified in both channel and pipe flows. The analysis reveals that the balance breaking and exchange of leading order terms in the mean energy equation that occurs across an intermediate layer is similar to the exchange of terms in the mean momentum equation. The present analysis suggests that, at high Peclet numbers in the four layer regime, the scaling characteristics of the temperature field become increasingly similar to those of the momentum field at high Reynolds number. The intermediate normalisation found by adopting the theory used for the momentum field provides a convincing scaling for the mean temperature and turbulent heat flux profiles for both pipe and channel flows. In contrast to velocity field statistics, the inner normalized mean temperature and heat flux profiles show significant discrepancies between pipe and channel flows.

1. Introduction

While velocity-statistical comparisons between pipe and channel flow are relatively commonplace, comparisons of thermal field statistics are not. An example comparison of velocity statistics is that Monty et al. [1] revealed long meandering features of wall-bounded turbulent pipe and channel flows. Later, Monty et al. [2] made comparisons of mean statistics of pipe and channel flows and found that the inner-normalized mean velocity profile was identical in these two flows for $y/\delta < 0.25$, where y is the wall normal distance and δ is the channel half-height or pipe radius. Higher order statistics such as skewness and flatness showed agreement that extended up to $y/\delta = 0.5$. Recent analyses of turbulent wall bounded flow in pipes and channels by Monty et al. [1,2], Wei et al. [3,4], Ng et al. [5], Chin [6] suggest that many of the statistical properties of these flows are similar, even though their geometries differ. At a nominally similar Reynolds number ($Re_\tau = \delta^+ = u_\tau\delta/\nu \simeq 1000$, where u_τ is the friction velocity and ν is the kinematic viscosity), Chin [6] performed a detailed comparative study of turbulent pipe and channel flow using DNS. He concluded that lower order statistics were more inclined to show agreement between the two different flows. The mean velocity profile of pipe flow, however, has a more pronounced wake function. Chin [6] further found good agreement of the Reynolds stress profiles of these two flows except beyond the logarithmic region ($y^+ \gtrsim 0.15Re_\tau$, where $y^+ = yu_\tau/\nu$ is the inner normalized wall-normal distance). His results suggest that the difference is mainly due to the constriction of the growth of structures in the azimuthal direction for the pipe flow. His investigations, however, did not examine the invariant scaling characteristics of pipe and channel flows.

Wei et al. [3] explored the four-layer structure of turbulent pipe and channel flows associated with the properties of the mean momentum equation. Based on a generic first-principles framework, Wei et al. [4] introduced a mesoscaling of Reynolds shear stress in turbulent channel and pipe flows that showed invariant profiles of shear stress. Further investigations by Klewicki et al. [7] and Klewicki [8] confirmed the identical behaviour of these two flows. This is reasoned to stem from these flows having identical mean dynamical equations. The value of Reynolds number at which the four layer structure is nominally established has been investigated for both channel and pipe flows [7,9], and in each case was found to be $Re_\tau \simeq 180$.

* Corresponding author. Tel.: +61 3 8344 6748; fax: +61 3 8344 4290.
E-mail addresses: sumons@student.unimelb.edu.au (S. Saha), klewicki@unimelb.edu.au (J.C. Klewicki), a.ooi@unimelb.edu.au (A.S.H. Ooi), hugh.blackburn@monash.edu (H.M. Blackburn).

http://dx.doi.org/10.1016/j.ijthermalsci.2014.10.010
1290-0729/

There are a large number of studies available to explore the various theories pertaining to the logarithmic-like properties of the mean velocity profile, including the von Kármán constant. In contrast, there is a relative paucity of data sets for wall bounded turbulent heat transfer. Efforts to explore the logarithmic-like properties of the mean temperature profile constitutes a long-standing challenge [10], owing to the complicated effects of both Reynolds number, Re_τ and Prandtl number, Pr. Analogous to the mean velocity profile, the logarithmic equation for the mean temperature profile in statistically stationary wall-bounded flow with turbulent heat transfer is traditionally written as

$$\overline{\Theta}^+ = \kappa_\theta^{-1}\ln y^+ + \beta(Pr), \tag{1}$$

where $\overline{\Theta}^+$ is the non-dimensional mean temperature normalized by the friction temperature, $T_\tau = q_w/\rho C_p u_\tau$, q_w is the heat flux applied at the wall, ρ is the mass density, C_p is the specific heat at constant pressure, κ_θ is the von Kármán constant for temperature, and β is an additive constant that has been purported to be directly proportional to Prandtl number and independent of Reynolds number [10]. Similar to what is found for the mean velocity profile, (1) is typically said to be valid on the region that is neither close to the wall nor near the centre of the pipe or channel. The thickness of the logarithmic layer depends on the magnitude of Reynolds and Prandtl numbers. Gowen and Smith [10] reported that the value of κ_θ^{-1} is almost constant at 2.5 for Prandtl numbers $0.026 \le Pr \le 14.3$ and Reynolds numbers $10^4 \le Re_\tau \le 5\times 10^4$. Kader [11] developed a correlation for the mean temperature profile based on interpolation of experimental data for both turbulent pipe and channel flow. Here the value of κ_θ^{-1} was set at 2.12. Kader's correlation is given by

$$\overline{\Theta}^+ = Pr\, y^+ \exp(-\Gamma) + \left[\kappa_\theta^{-1}\ln\left\{\left(1+y^+\right)\frac{1.5(2-y/\delta)}{1+2(1-y/\delta)^2}\right\} + \beta(Pr)\right]\exp(-1/\Gamma), \tag{2}$$

where

$$\Gamma = \frac{10^{-2}\left(Pr\, y^+\right)^4}{1+5Pr^3\, y^+} \text{ with } \kappa_\theta^{-1} = 2.12. \tag{3}$$

Kader also established an approximate form for the additive function, $\beta(Pr)$, that determines the temperature difference between the wall and the lower edge of the logarithmic layer as follows

$$\beta(Pr) = \left(3.85Pr^{1/3} - 1.3\right)^2 + \kappa_\theta^{-1}\ln(Pr). \tag{4}$$

Table 1
List of the values of von Kármán constant κ_θ for turbulent heat transfer.

References	Type	Re_τ	Pr	$Pe_\tau = Re_\tau Pr$	κ_θ
Kasagi et al. [12]	Channel	150	0.71	106.5	0.36
Johansson and Wikström [13]	Channel	265	0.71	188.15	0.33
Kawamura et al. [14]	Channel	180–395	0.2–0.71	36–280.45	0.40
Kawamura et al. [15]	Channel	180–395	0.2–1.0	36–395	0.41
Kawamura and Abe [16]	Channel	180–640	0.71	127.8–454.4	0.43
Orlandi and Leonardi [17]	Channel	180–395	1.0	180–395	0.41
Abe et al. [18]	Channel	180–1020	0.71	127.8–724.2	0.43
Piller [19]	Pipe	180	0.71	127.8	0.34
Satake et al. [20]	Pipe	180	0.71	127.8	0.35
Satake et al. [20]	Pipe	1050	0.71	745.5	0.46
Redjem-Saad et al. [21]	Pipe	186	0.2–1.0	37.2–186	0.347

This equation is reported to be valid for Pr number ranging from 6×10^{-3} to 40×10^3. Data from DNS can be used to provide an estimate (albeit at low Re_τ) for the value of κ_θ in the logarithmic region. Table 1 shows a representative list of studies along with their estimated values of κ_θ.

The significance of a universal κ_θ in the logarithmic law is expressed by the slope of the mean temperature profile and is reflected by the weighted wall-normal gradient of $\overline{\Theta}^+$ such as $\kappa_\theta = (y^+ d\overline{\Theta}^+/dy^+)^{-1}$. Applied engineering practice often assumes that κ_θ is a constant in order to estimate the mean temperature profile, and thus to find the effective thermal efficiency. Empirical evidence, however, shows that κ_θ varies with the type of flow and with Reynolds and Prandtl numbers (see Table 1). Moreover, some researchers, such as George [22], argue that neither theory nor the data support the existence of a universal log law for wall-bounded turbulent flows. The variation of κ_θ in Table 1 motivates a more detailed analysis.

As noted at the outset, comparative studies of turbulent heat transfer in pipes and channels are rare. Kozuka et al. [23] compared mean temperature profiles obtained from channel DNS with Kader's correlation [11]. They found that (2) predicted the mean profile reasonably for $Re_\tau = 395$, but with increasing Pr the differences in the logarithmic region became significant. Only Piller [19]; Satake et al. [20] and Redjem-Saad et al. [21] have attempted to make a comparison between turbulent pipe and channel flow DNS. Redjem-Saad et al. [21] compared RMS temperature fluctuations and turbulent heat flux for $0.026 \le Pr \le 1.0$ at $Re_\tau = 186$ with the channel flow DNS data of Kawamura et al. [24]. Both Redjem-Saad et al. [21] and Satake et al. [20] calculated the turbulent Prandtl number profile. Their results showed agreement with Kawamura et al. [24] in the vicinity of the wall. Neither of these works compared the scaling properties of the thermal energy equation for these two different geometries, as is done herein.

Investigations of thermal scaling analysis have been carried out for the case of channel flow [25–28]. A brief review is presented in Saha et al. [28]. In contrast, no detailed thermal scaling analyses have been conducted for pipe flow. This at least partly stems from the limited availability of data sets for turbulent heat transfer in pipe flow. Our present efforts place attention on revealing the scaling properties of the mean energy equation for the case of turbulent heat transfer in pipe flow. DNS for a range of moderate Reynolds and Prandtl numbers are carried out and compared with existing channel data. The present analysis follows the framework explained in Saha et al. [28]. Properties of four distinct thermal balance layers and a generalized form of the intermediate length scaling are utilized to reveal the subtle differences and highlight the similarities between the pipe and channel statistics.

2. Simulation procedure

2.1. Mathematical model

Direct numerical simulation was carried out for flow in a heated pipe of radius δ and length L. The velocity field is turbulent and fully-developed. The incompressible Newtonian fluid is heated with a uniform heat flux q_w imposed at the pipe wall. The fluid properties are assumed to be constant and the temperature is treated as a passive scalar. The three-dimensional incompressible Navier–Stokes equations in cylindrical coordinates can be written as

$$\frac{\partial \mathbf{u}}{\partial t} + N(\mathbf{u}) = -\nabla P' + \nu\nabla^2\mathbf{u} + \mathbf{F}, \tag{5}$$

$$\nabla\cdot u = 0, \tag{6}$$

where $P' = p'/\rho$ is the kinematic fluctuating pressure, $N(\mathbf{u})$ represents the non-linear advection terms implemented in skew-symmetric form for robustness and the velocity vector is $\mathbf{u}(x,r,\theta,t) = (u_x,u_r,u_\theta)$. Coordinates in the axial, radial and azimuthal directions are denoted by x, r, θ respectively. The last term in Equation (5) is the forcing vector $\mathbf{F} = (F_x,0,0)$, where $F_x = 2u_\tau^2/\delta$ is the axial driving force per unit mass that corresponds to the mean pressure gradient in the x-direction. Its use allows both the pressure and velocities to remain axially periodic. We consider no-slip boundary conditions for all velocity components, and Neumann boundary conditions for the pressure at the pipe wall.

The energy equation for passive scalar (temperature) transport is

$$\frac{\partial T}{\partial t} + N(T) = \alpha\nabla^2 T, \tag{7}$$

where $N(T)$ represents the non-linear thermal advection terms in skew-symmetric form, $\alpha = k_c/\rho C_p$ is the thermal diffusivity and k_c is the thermal conductivity. The temperature field is fully developed (see below), and thus statistically homogeneous in the axial direction. Periodic boundary conditions are used in the axial direction for the temperature field.

Based on the unit length scale and the unit velocity scale, the governing Equations (5)–(7) can be transformed to dimensionless equations in a number of ways. There are two different approaches that are usually employed. In the first approach, the fundamental length scale is the pipe diameter, $D = 2\delta$, and the unit velocity scale is the bulk-flow velocity u_b, which is defined as the ratio of mean volumetric flow rate and pipe cross-sectional area ($4\langle Q\rangle/\pi D^2$). The time scale is therefore D/u_b. After normalization, (5) becomes

$$\frac{\partial \mathbf{U}}{\partial t_b} + N(\mathbf{U}) = -\nabla P_b' + \frac{1}{Re_D}\nabla^2\mathbf{U} + \overline{\mathbf{F}}, \tag{8}$$

where $\overline{\mathbf{F}} = (16Re_\tau^2/Re_D^2, 0, 0)$ and $Re_D = u_b D/\nu$ is the bulk-flow Reynolds number. In order to calculate the required dimensionless axial force term, one has to estimate the value of Re_τ. One of the common methods is to use the Blasius relationship [29] for turbulent flow in a smooth pipe. At moderate Reynolds numbers ($2500 \le Re_D \le 10^5$), the Blasius law [29] for the smooth-pipe relationship is given by

$$Re_\tau = 99.436 \times 10^{-3} Re_D^{7/8}. \tag{9}$$

The dimensionless temperature Θ is traditionally defined as

$$\Theta = \frac{\langle T_w\rangle - T}{T_r}, \tag{10}$$

where $T_r = q_w/\rho C_p u_b$ is a reference temperature based on bulk velocity and $\langle T_w\rangle$ denotes the wall temperature averaged in time and in the circumferential direction. Normalization of (7) using these variables yields

$$\frac{\partial \Theta}{\partial t_b} + \mathbf{U}.\nabla\Theta - U_x\frac{1}{T_r}\frac{\partial\langle T_w\rangle}{\partial X} = \frac{1}{Re_D Pr}\nabla^2\Theta, \tag{11}$$

where $Pr = \nu/\alpha$ is the Prandtl number and $X = x/D$ is the nondimensional distance in streamwise direction. Due to axial periodicity of the temperature field, the rate of change of ensemble-averaged temperature becomes invariant. The wall thermal boundary condition demands a linear increase of the bulk temperature $\langle T_b\rangle$ in the axial direction. The following equalities are satisfied for thermally fully developed flows,

$$\frac{\partial\langle T\rangle}{\partial X} = \frac{\partial\langle T_b\rangle}{\partial X} = \frac{\partial\langle T_w\rangle}{\partial X} = \text{constant}, \tag{12}$$

and by adopting the mean energy balance for the current problem, one can show that

$$\frac{\partial\langle T_w\rangle}{\partial X} = \frac{4q_w}{\rho C_p u_b} = 4T_r. \tag{13}$$

The dimensionless energy Equation (11) can be written as

$$\frac{\partial\Theta}{\partial t_b} + \mathbf{U}.\nabla\Theta - 4U_x = \frac{1}{Re_D Pr}\nabla^2\Theta. \tag{14}$$

This approach of nondimensionalization is employed in the studies by McIver et al. [30]; Chin et al. [31,32] for the velocity field, and by Saha et al. [33] for thermal field. One needs a good estimate of the Reynolds number Re_τ (e.g., from an available correlation) in order to fix the axial force term. This limitation can be overcome by using the wall friction velocity, u_τ, to normalize (5)

$$\frac{\partial\mathbf{u}^+}{\partial t_\tau} + N(\mathbf{u}^+) = -\nabla P'^+ + \frac{1}{2Re_\tau}\nabla^2\mathbf{u}^+ + \overline{\mathbf{F}}^+, \tag{15}$$

where $\overline{\mathbf{F}}^+ = (4,0,0)$. Similarly, the thermal energy equation can be normalised using the friction temperature, T_τ, and then (7) takes the form

$$\frac{\partial\Theta^+}{\partial t_\tau} + \mathbf{u}^+.\nabla\Theta^+ - 8\frac{Re_\tau}{Re_D}u_x^+ = \frac{1}{2Re_\tau Pr}\nabla^2\Theta^+. \tag{16}$$

One needs Re_D in advance in order to integrate (16), i.e., the solution to the Navier–Stokes Equation (15) needs to have reached a statistically steady state in order to evaluate Re_D, and thus maintain a constant ensemble-averaged temperature at each point. Using normalised variables, the thermal boundary condition at the wall is

$$\Theta = \Theta^+ = 0. \tag{17}$$

In the present study, the governing Equations (15) and (16) are considered, as this avoids the need for any empirical correlation to estimate the required parameters.

2.2. Numerical method

The present DNS code is based on a cylindrical-coordinate spectral element/Fourier spatial discretization technique [34] that can solve the governing Equations (15) and (16) with high spatial accuracy. The spatial discretisation employs two-dimensional spectral element mesh in the meridional semi-plane and Fourier expansion in the azimuthal coordinate. Within each spectral element 10th order Gauss–Lobatto–Legendre Lagrange interpolants are employed. Exponential or spectral convergence can be achieved through this method and it has successfully been used for DNS of turbulent heat transfer in pipe flow [33]. Turbulent flow is computed from an initial velocity and pressure field supplied by the fully developed flow state obtained by Chin [6], while the initial thermal field is given as the streamwise velocity component multiplied by the Prandtl number. Simulations are carried out until the ensemble average temperature at the centre of the pipe has converged to a constant value. The validation of flow field and thermal statistics has been successfully carried out in order to gain confidence in the accuracy of the statistics. The validation procedures and the comparative results are documented by Saha [35].

3. Datasets

Thermal statistics of pipe flow are derived from the DNS just described. Channel flow data were gathered from the open literature. Momentum analyses indicate that the onset of the four layer structure for pipe flow occurs at about $Re_\tau = 180$ [7]. Thus, the parameter range of the present experiments allows comparison of these two flows for a Reynolds number fixed near the onset of the four layer regime for the momentum field. The influence of different domain lengths on the accuracy of the various thermal statistics was investigated and described in Saha et al. [33]. Here, we present results from numerical simulations for $Pr = 0.025–0.71$ in a pipe of length $L/\delta = 8\pi$ and $Pr = 1–7$ for $L/\delta = 4\pi$ at $Re_\tau = 180$. A pipe length of $L = 8\pi\delta$ was selected for all simulations at $Re_\tau = 395$. This selection is a compromise between the required computational cost and the accuracy of various thermal statistics. Table 2 shows the simulation parameters and grid resolutions for the present data sets. For each data set, the statistics were calculated after the flow had reached a statistically steady state. High resolution DNS data of turbulent channel flow and heat transfer from Kawamura's group [23,24,36] for $0.025 \le Pr \le 7$ and $Re_\tau = 180$ and 395 are also shown for comparison. It should be noted here that the same thermal boundary condition (isoflux heating) for channel flow DNS is used in the present pipe flow simulations.

4. Mean thermal energy equation

A rational starting point for scaling analysis of heat transfer is the mean thermal energy equation. The companion analysis associated with heat transfer in fully developed turbulent channel flow has been presented in detail in Saha et al. [28]. As a result, we only consider the case of pipe flow, and then compare with the channel flow equation. We consider statistically stationary flow and heat transfer in an axisymmetric pipe. By applying Reynolds decomposition and time averaging (7) becomes

$$\overline{u}_x\frac{\partial\overline{T}}{\partial x} = \alpha\left[\frac{\partial^2\overline{T}}{\partial x^2} + \frac{1}{r}\frac{\partial}{\partial r}\left(r\frac{\partial\overline{T}}{\partial r}\right)\right] - \frac{1}{r}\frac{\partial\left(r\langle u_r'T'\rangle\right)}{\partial r}, \tag{18}$$

where $\overline{u}_x$ is the streamwise mean velocity, $\overline{T}$ is the mean temperature, u_r' is the fluctuating radial velocity and T' is the fluctuating temperature. The expression for the mean axial temperature gradient (13) allows (18) to be written as

$$\frac{2q_w\overline{u}_x}{\rho C_p u_b\delta} = \frac{\nu}{rPr}\frac{\partial}{\partial r}\left(r\frac{\partial\overline{T}}{\partial r}\right) - \frac{1}{r}\frac{\partial\left(r\langle u_r'T'\rangle\right)}{\partial r}. \tag{19}$$

The boundary conditions at the pipe wall, $r = \delta$, are

$$\overline{u}_x = u_r' = T' = 0, \frac{\partial\overline{T}}{\partial r} = \frac{q_w}{k_c}. \tag{20}$$

This implies that there are no fluctuating components of streamwise velocity and temperature at the wall. At the centreline, $r = 0$,

$$\frac{\partial\overline{T}}{\partial r} = \langle u_r'T'\rangle = 0. \tag{21}$$

Integrating (19) with respect to r from the pipe centre ($r = 0$) to some arbitrary r ($r < \delta$) and making use of the boundary conditions (21) yields

$$\frac{2q_w}{\rho C_p u_b r\delta}\int_0^r r\overline{u}_x dr = \frac{\nu}{Pr}\frac{\partial\overline{T}}{\partial r} - \langle u_r'T'\rangle. \tag{22}$$

It is convenient to rewrite (19) in terms of the distance from the wall, $y = \delta - r$. Using this and (22) yields

$$\frac{2q_w}{\rho C_p u_b\delta}\left[\frac{1}{(y-\delta)^2}\int_\delta^{\delta-y}(y-\delta)\overline{u}_x dy - \overline{u}_x\right] = \frac{\nu}{Pr}\frac{\partial^2\overline{T}}{\partial y^2} - \frac{\partial\langle u_r'T'\rangle}{\partial y}, \tag{23}$$

where the bulk velocity can be expressed as

$$u_b = \frac{2}{\delta^2}\int_0^\delta(\delta-y)\overline{u}_x(y)dy. \tag{24}$$

By employing the non-dimensional mean temperature variable, $\overline{\Theta}^+$, the inner normalized form of (23) becomes

$$\frac{1}{Pr}\frac{d^2\overline{\Theta}^+}{dy^{+2}} + \frac{d\overline{T}_\theta^+}{dy^+} + \varepsilon^2 R_s\left(y^+\right) = 0, \tag{25}$$

where $R_s(y^+) = 2/u_b^+[1/(y^+-\delta^+)^2\int_{\delta^+}^{\delta^+-y^+}(y^+-\delta^+)\overline{u}_x^+ dy^+ - \overline{u}_x^+]$ is the scaled thermal advection function, $\delta^+ = Re_\tau$, $\varepsilon = 1/\sqrt{\delta^+}$ and $\overline{T}_\theta^+ = -\langle u_r'T'\rangle^+$ is the inner normalized radial turbulent heat flux. Similarly, the outer normalised form of (18) becomes

$$\frac{\varepsilon^2}{Pr}\frac{d^2\overline{\Theta}^+}{d\eta^2} + \frac{d\overline{T}_\theta^+}{d\eta} + R_s(\eta) = 0, \tag{26}$$

where $R_s(\eta) = 2/u_b[1/(\eta-1)^2\int_1^{1-\eta}(\eta-1)\overline{u}_x d\eta - \overline{u}_x]$ and $\eta = y/\delta$ is the outer normalized wall normal distance. Equations (25) and (26) are analogous to the mean energy equations for channel flow [28]

Table 2
Summary of comparison of DNS database for turbulent heat transfer in channel and pipe flow. Pipe flow data is obtained from the present DNS whereas channel flow data is adopted from the DNS database of Kawamura's group [23,24,36] at http://murasun.me.noda.tus.ac.jp/turbulence/poi/poi.html.

Flow type	Re_τ	Pr	Pe_τ	L/δ	Δx^+	Δy^+	$\Delta z^+/\Delta(\delta\theta)^+$	Symbol
Channel	180	0.025	4.5	12.8	9.0	0.20–5.90	4.5	⊗
Pipe	180	0.025	4.5	8π	9.0	0.178–5.589	4.4	©
Channel	180	0.05	9	6.4	9.0	0.4–11.5	4.5	✷
Pipe	180	0.05	9	8π	9.0	0.178–5.589	4.4	♠
Channel	180	0.1	18	6.4	9.0	0.4–11.5	4.5	■
Pipe	180	0.1	18	8π	9.0	0.178–5.589	4.4	□
Channel	180	0.2	36	6.4	9.0	0.4–11.5	4.5	♣
Pipe	180	0.2	36	8π	9.0	0.178–5.589	4.4	⌀
Channel	180	0.4	72	6.4	9.0	0.4–11.5	4.5	★
Pipe	180	0.4	72	8π	9.0	0.178–5.589	4.4	⊕
Channel	180	0.6	108	6.4	9.0	0.4–11.5	4.5	▼
Pipe	180	0.6	108	8π	9.0	0.178–5.589	4.4	▽
Channel	180	0.71	127.8	6.4	1.1	0.05–0.97	1.1	●
Pipe	180	0.71	127.8	8π	9.0	0.178–5.589	4.4	○
Channel	180	1.0	180	6.4	1.1	0.05–0.97	1.1	▶
Pipe	180	1.0	180	4π	4.5	0.06–3.73	4.4	▷
Channel	180	2.0	360	6.4	1.1	0.05–0.97	1.1	◆
Pipe	180	2.0	360	4π	4.5	0.06–3.73	4.4	◇
Channel	180	5.0	900	6.4	4.5	0.20–5.90	2.25	▲
Pipe	180	5.0	900	4π	4.5	0.02–1.65	2.2	△
Channel	180	7.0	1260	6.4	0.56	0.05–0.97	1.1	◀
Pipe	180	7.0	1260	4π	4.5	0.02–1.65	2.2	◁
Channel	395	0.025	9.875	12.8	9.88	0.15–6.52	4.94	⊗
Pipe	395	0.025	9.875	8π	9.9	0.13–8.2	4.85	©
Channel	395	0.71	280.45	6.4	1.2	0.11–2.1	2.5	•
Pipe	395	0.71	280.45	8π	9.9	0.04–3.6	4.85	○
Channel	395	1.0	395	6.4	1.2	0.11–2.1	2.5	▶
Pipe	395	1.0	395	8π	9.9	0.04–3.6	4.85	▷

except the expressions for $\overline{T}_\theta^+$ and R_s are for a circular geometry.

For future reference, we also note that the formulation of Wei et al. [25] provides an alternate form of the inner normalised energy equation

$$\frac{d^2\psi}{dy_\sigma^2} + \frac{d\overline{T}_\theta^+}{dy_\sigma} + \sigma^2 R_\sigma(y_\sigma) = 0, \qquad A + B + C = 0 \tag{27}$$

where $\psi = \overline{\Theta}^+/\overline{\Theta}^+|_{\eta=1}$, $\sigma^2 = \overline{\Theta}^+|_{\eta=1}/(Pr\delta^+)$, $y_\sigma = \eta/\sigma^2$ is the new inner normalized distance and the scaled advection function is $R_\sigma(y_\sigma) = R_s(\eta(y_\sigma)) = R_s(\sigma^2 y_\sigma)$. The boundary conditions on (27) are

$$\psi = \overline{T}_\theta^+ = 0, \ \frac{d\psi}{dy_\sigma}(0) = 1 \quad \text{at} \quad y_\sigma = 0. \tag{28}$$

An alternate inner variable is introduced here to identify the dependences on Pr and it can be expressed by assuming the power law effect of Prandtl number as

$$y_\theta^+ = Pr^b y^+, \tag{29}$$

where b is a constant coefficient. Employing it in (25) yields

$$\frac{d^2\overline{\Theta}^+}{dy_\theta^{+2}} + \frac{d\overline{T}_\phi^+}{dy_\theta^+} + \phi^2 R_\theta\left(y_\theta^+\right) = 0, \qquad A + B + C = 0 \tag{30}$$

where $R_\theta(y_\theta^+) = R_s(\eta(y_\theta^+)) = R_s(Pr^{-b} y_\theta^+/\delta^+)$, $\overline{T}_\phi^+ = Pr^{1-b}\overline{T}_\theta^+$ and $\phi = 1/\sqrt{\delta^+ Pr^{2b-1}}$. The thermal boundary conditions at the pipe wall, $y_\theta^+ = 0$, are

$$\overline{\Theta}^+ = 0, \ \frac{d\overline{\Theta}^+}{dy_\theta^+} = Pr^{1-b}. \tag{31}$$

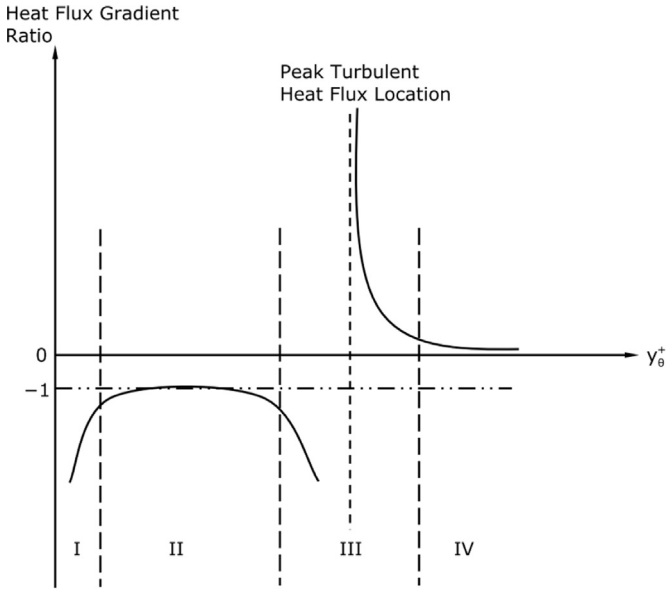

Fig. 1. Sketch of the four layers structure of the leading terms in (30) for fixed Peclet number; layer I is the molecular diffusion/mean advection balance layer, layer II is the heat flux gradient balance layer, layer III is the heat flux gradient/mean advection balance meso layer and layer IV is the turbulent heat flux gradient/mean advection balance layer. Note that across layer III the turbulent heat flux gradient crosses through zero, and there is an exchange of leading order balance.

At sufficiently high Re_τ, $R_\theta(y_\theta^+)$ is $O(1)$ for all values of y_θ^+ except in the region interior to the peak in the Reynolds shear stress. Note also that (27) and (30) are governed by three mechanisms; A = gradient of the molecular diffusion flux, B = gradient of the turbulent transport flux and C = mean streamwise advection.

5. Thermal scaling characteristics

During the transitional regime in the channel, the balance of leading order terms in the mean energy equation has yet to organize into the distinct four layer structure [28]. A representative smooth-wall four layer thermal structure at a fixed Peclet number is illustrated in Fig. 1 based on the ratio of the heat flux gradients (A/B in (27) or (30)). Within each layer the terms in (27) or (30) are not all of leading order. The magnitude of the ratio (A/B) exceeds unity in layer I, indicating a nominal balance between the mean streamwise advection and the gradient of molecular diffusion flux, and thus coincides with the traditional conductive sublayer. In layer II, the dominant balance is between the gradient of the molecular diffusion flux and turbulent transport flux. All three terms are of equal order across layer III, whereas the A term loses leading order and there exists a dominant balance between the B and C terms in layer IV. Here we investigate the proposed scalings (described in Saha et al. [28] for channel flow) associated with thermal four layer structure of pipe flow.

5.1. Minimum Prandtl number

The magnitude orderings of terms A, B and C in (27) and (30) are used to explore the Re_τ and Pr dependencies on the formation of the four layer regime, see [28]. Here it is useful to reiterate that the scaled advection function (term C), although distinct from the channel flow case, approaches a constant in the outer region for increasing Re_τ and fixed Pr, and that the onset of the four layer regime for momentum occurs at nominally the same Reynolds number $Re_\tau = 180$ for both pipe and channel flows [7,9].

By examining the ratio of terms A/B as shown in Fig. 2(a), we can explore the onset of the four layer regime for the thermal field in pipe flow. Here the aim is to determine the minimum Prandtl number for the existence of the thermal four-layer structure for Re_τ at least at the onset of the four-layer regime for the momentum field. Using the criterion based on the ordering of terms in layers II and IV, we estimate the lowest value of Pr for $Re_\tau \geq 180$ that satisfies the thermal four-layer structure. In order to satisfy the criteria proposed by Elsnab et al. [9], the ordering of the terms A, B and C should be such that $|B/C|_{\max} \geq 10$ in layer II and $|B/A|_{\max} \geq 10$ in layer IV. A close examination of Fig. 2(a) for $Pr < 0.6$ reveals that in layers II and III these criteria are not simultaneously met. At $Pr \sim 0.6$, however, $|B/C|$ attains a maximum value of 14.6 in layer II and $|B/A|_{\max} \simeq 11.23$ in layer IV. This confirms that, similar to channel flow, the onset of the four layer thermal regime occurs for $Pr \geq 0.6$ at $Re_\tau \simeq 180$.

5.2. The four layer regime

Fig. 2(b) plots the heat flux gradient ratio (A/B) as a function of $y_\theta^+ = Pr\, y^+$ for $Pr \geq 0.6$. It exhibits the distinct four-layer structure also found in channel flow. In layer I, however, this ratio attains large negative values for low Pr. This is different from the channel, e.g., see Fig. 5(d) in Saha et al. [28]. For increasing Prandtl number, the beginning of layer II moves to smaller y_θ^+. As expected, the outer edge of the -1 ratio region moves to greater y_θ^+ with increasing Reynolds and Prandtl numbers. Around the location of the peak turbulent heat flux, there is a balance breaking and exchange process where all three terms are of the same order (layer III). The

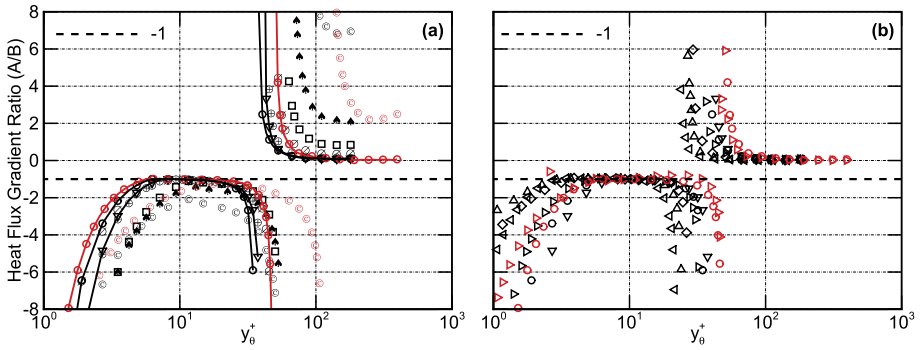

Fig. 2. Ratio of the gradient of the molecular diffusion flux to the gradient of the turbulent transport flux (A/B) in pipe flow. Symbol shapes for DNS data are given in Table 2. (a) The solid lines mark data for $Pr \geq 0.6$. The wall normal distance y_θ^+ is chosen as y^+ for the case at $b = 0$ (see Equation (29)). (b) Results are from the present proposal of (30) for $b = 1$ and $Pr \geq 0.6$. All black symbols represent data for $Re_\tau = 180$ and red symbols for $Re_\tau = 395$. (For interpretation of the references to colour in this figure legend, the reader is referred to the web version of this article.)

dynamical characteristics of layer III leads one to consider how to best express the mean energy equation in an invariant form that properly reflects this leading order balance. The last layer (layer IV) clearly shows that the leading balance here is between the gradients of turbulent heat flux and the streamwise mean advection.

6. Comparison of inner and outer scaling

6.1. Mean temperature profiles

The conventional way to represent the mean temperature near the wall involves normalization using the friction temperature and the viscous length scale, e.g., [19,21,23]. Fig. 3 compares the inner-normalised mean temperature between pipe and channel flows. The influences of Prandtl and Reynolds numbers are separately marked in Fig. 3(a) and (b). Apart from a narrow zone within the molecular sublayer (layer I), the mean temperature profiles do not merge anywhere for varying Pr, see Fig. 3(a). An underlying reason for this is that the normalisation parameter does not include the effect of Prandtl number explicitly. This point is clarified in Fig. 3(b), which shows that the traditional inner normalization works well in layer I (at least) for fixed Prandtl number.

A noticeable difference between the pipe and channel flow temperature profiles is apparent in the logarithmic layer at higher Prandtl numbers. Here, there is a tendency for pipe flows to have a higher normalized temperature. This observation is consistent with the findings of Piller [19]. A similar observation was also noted by Chin [6] when comparing the streamwise mean velocity in pipes and channels, where the pipe mean velocity profile exhibited a larger wake function. Comparison of the mean temperature in the pipe and channel (Fig. 3) reveals that Kader's correlation fails to merge the mean temperature profiles of both pipe and channel flows, irrespective of variations in Reynolds and Prandtl numbers.

The shortcoming of the traditional inner scaling near the wall can be addressed by an alternate scaling based on a Taylor series expansion of the mean temperature profile. The resulting normalised mean temperature depends on Prandtl number and was employed by Redjem-Saad et al. [21] for pipe flow and Kawamura et al. [24], Abe et al. [37], Kawamura et al. [38] for channel flow. This alternate normalization for the mean temperature, $\overline{\Theta}^+/Pr$, is shown in Fig. 4(a). Emphasis is on the vicinity of the wall, where the profile displays an asymptotic behaviour within the conductive sublayer for both pipe and channel flows. Using a $Pr-$ dependent thermal length scale with an exponent b, the proposed inner scaling (30) also yields invariant mean temperature profiles near the wall for both pipe and channel flows. Here the value of the coefficient b is set to 1 based upon the parametric investigation performed by Saha et al. [28]. The proposed scaling is illustrated in Fig. 4(b). This normalisation yields profiles very similar to the alternate normalization, but without altering the value of the mean temperature. Under the current scaling framework, both pipe and channel flow data show marginal deviations in the mean temperature profiles for higher Pr and Re_τ.

The inner normalised mean temperature that follows the formulation of Wei et al. [25] as mentioned in (27) is illustrated in Fig. 5. Near the wall, the comparison between pipe and channel

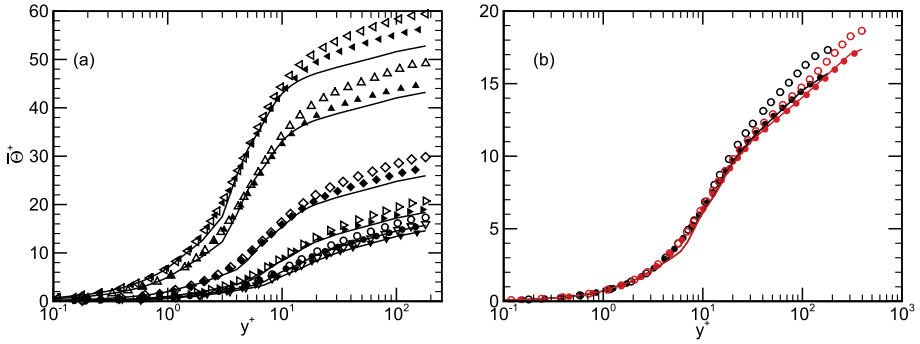

Fig. 3. Comparison of traditional inner scaling of mean temperature for pipe and channel showing effect of (a) Prandtl numbers at $Re_\tau = 180$ and (b) Reynolds numbers at $Pr = 0.71$. The upward shifted data shown in (a) has higher value of Pr. Symbol shapes for DNS data are given in Table 2. The solid lines show temperature profiles from Kader's correlation [11]. All black symbols/lines represent data for $Re_\tau = 180$ and red symbols/lines for $Re_\tau = 395$. (For interpretation of the references to colour in this figure legend, the reader is referred to the web version of this article.)

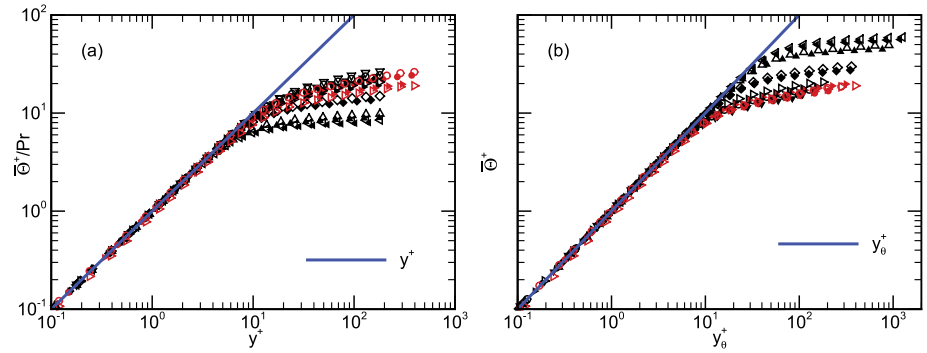

Fig. 4. Comparison of inner scaling of mean temperature for pipe and channel. (a) Alternate inner scaling and (b) proposed inner scaling (30) for $b = 1$. Symbol shapes for DNS data are given in Table 2. All black symbols represent data for $Re_\tau = 180$ and $0.6 \le Pr \le 7.0$, and red symbols for $Re_\tau = 395$ and $Pr = 0.71, 1.0$. (For interpretation of the references to colour in this figure legend, the reader is referred to the web version of this article.)

flows yields a convincing profile invariance. In the outer part, the change of Reynolds number, however, separates the temperature profiles showing the existence of logarithmic region of the normalised mean temperature. Furthermore, the variation of Prandtl number does not show any impact on the mean temperature near the wall. This is seen by observing the profiles for the black symbols ($Re_\tau = 180$) and the red symbols ($Re_\tau = 395$).

Although the traditional inner normalization of the mean temperature fails to scale the data properly, the outer-normalised mean temperature profiles appear to nominally exhibit invariance with both Pr and Re_τ for $\eta \gtrsim 0.2$. This is shown in Fig. 6, where the inner-normalized mean temperature is plotted in defect form.

6.2. RMS temperature profiles

The traditional inner and outer scaling of the root-mean-square (rms) temperature fluctuation is compared for channel and pipe flows in Fig. 7. This normalization fails to produce an invariant profile near the pipe or channel wall (see Fig. 7(a)). Fig. 7(b) shows that the peak of the temperature rms increases and moves to smaller y^+ with increasing Re_τ, and especially Pr (see also [14,21]). Interestingly, there exists a weak dependence on the flow configuration that is most easily seen at higher Re_τ and Pr. Both Piller [19] and Redjem-Saad et al. [21] compared the temperature rms profiles in pipe and channel flows. They observed that the rms of temperature fluctuation of pipe flow was slightly larger than that of channel flow in the region from the location of the peak to the axis of the pipe or channel. In fact, Redjem-Saad et al. [21] found that this behaviour was most strongly influenced by variations in Pr, as also observed in the present comparison.

The failure of inner-normalisation in Fig. 7 promotes the investigation of alternative normalizations. Taylor series expansions can be used to represent the temperature rms as $y \to 0$,

$$\overline{\Theta}'^{+} = Pr\left(b_\theta y^+ + c_\theta y^{+2} + \ldots\right), \tag{32}$$

see [14,21,24]. According to the prediction of Redjem-Saad et al. [21], b_θ should be independent of Pr if the Prandtl number is higher than a certain limiting value ($Pr \ge 0.71$ for $Re_\tau = 186$). Kawamura et al. [14,24] found an approximately constant value of the coefficient b_θ for $Pr \ge 0.2$. The logarithmic plot of $\overline{\Theta}'^{+}_{\mathrm{rms}}/Pr$ in Fig. 8(a) confirms the near-wall profile invariance for both pipe and channel flows. Our selection of data for $Pr \ge 0.6$ also shows that the value of b_θ is independent of Pr in the vicinity of the wall. Moreover, Kawamura et al. [14], Redjem-Saad et al. [21] employed the alternate normalization, $\overline{\Theta}'^{+}_{\mathrm{rms}}/Pr\ y^+$ versus y^+, in semi-logarithmic axes,

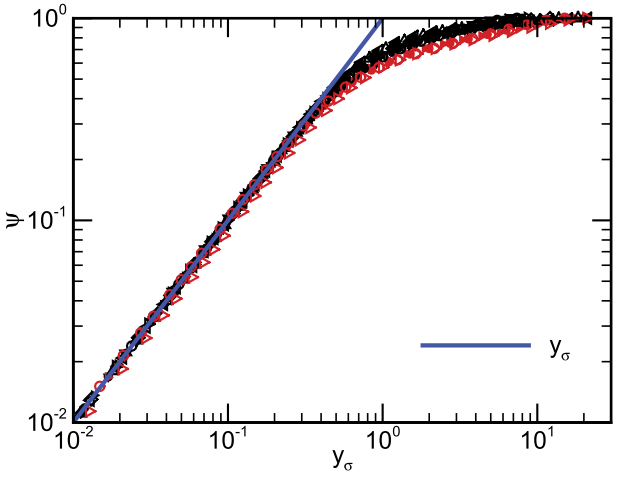

Fig. 5. Comparison of inner scaling of mean temperature for pipe and channel following Wei et al. [25] as mentioned in (27). Symbol shapes for DNS data are given in Table 2. All black symbols represent data for $Re_\tau = 180$ and $0.6 \le Pr \le 7.0$, and red symbols for $Re_\tau = 395$ and $Pr = 0.71, 1.0$. (For interpretation of the references to colour in this figure legend, the reader is referred to the web version of this article.)

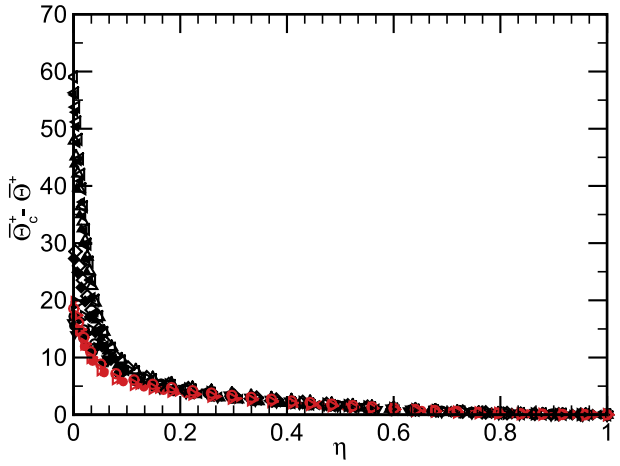

Fig. 6. Comparison of traditional outer scaling of mean temperature (temperature defect law) for pipe and channel. Symbol shapes for DNS data are given in Table 2. All black symbols represent data for $Re_\tau = 180$ and $0.6 \le Pr \le 7.0$, and red symbols for $Re_\tau = 395$ and $Pr = 0.71, 1.0$. (For interpretation of the references to colour in this figure legend, the reader is referred to the web version of this article.)

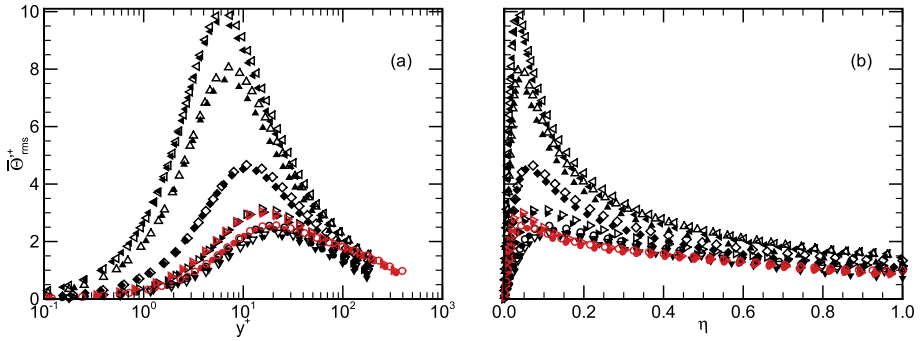

Fig. 7. Comparison of traditional (a) inner and (b) outer scaling of rms of temperature fluctuation for pipe and channel. Symbol shapes for DNS data are given in Table 2. All black symbols represent data for $Re_\tau = 180$ and $0.6 \leq Pr \leq 7.0$, and red symbols for $Re_\tau = 395$ and $Pr = 0.71, 1.0$. (For interpretation of the references to colour in this figure legend, the reader is referred to the web version of this article.)

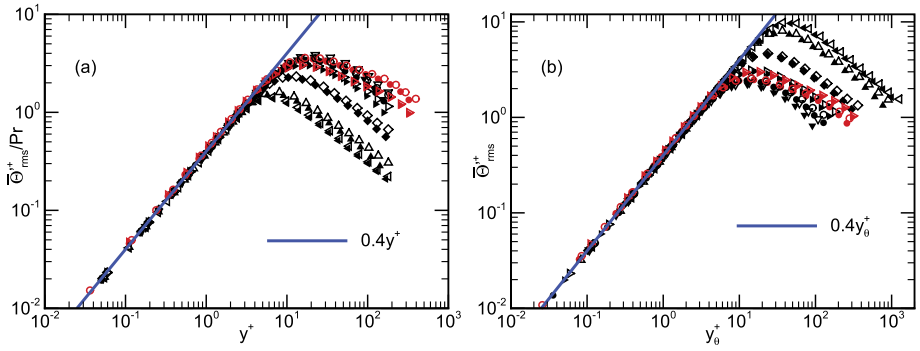

Fig. 8. Comparison of inner scaling of rms of temperature fluctuation for pipe and channel. (a) Alternate inner scaling (32) and (b) proposed inner scaling (30) for $b = 1$. Symbol shapes for DNS data are given in Table 2. All black symbols represent data for $Re_\tau = 180$ and $0.6 \leq Pr \leq 7.0$, and red symbols for $Re_\tau = 395$ and $Pr = 0.71, 1.0$. (For interpretation of the references to colour in this figure legend, the reader is referred to the web version of this article.)

which allowed them to easily determine the asymptotic value of b_θ as $y \to 0$. The value of the coefficient b_θ near the wall for pipe flow was estimated by Redjem-Saad et al. [21] to be approximately 0.4 for $Pr \geq 0.71$ at $Re_\tau = 186$, whereas Kawamura et al. [14] found a slightly lower value ($b_\theta \simeq 0.38$ at $Re_\tau = 180$) in the channel.

The proposed scaling (30) based on a Pr-dependent thermal length scale replicates a similar trend in the vicinity of the wall (see Fig. 8(b)). Like the proposed mean temperature profile (Fig. 4(b)), the influence of Reynolds and Prandtl number on the temperature rms is effectively removed near the wall. From this, we surmise that the proposed scaling approach (30) successfully satisfies the inner-normalisation requirements for both mean and fluctuating temperature and is applicable to both pipe and channel flows. Moreover, the present comparison between pipe and channel displays consistent, but not identical trends for all values of Pr and Re_τ. This is mainly due to the change of the duct curvature which affects the distribution of thermal boundary conditions, as explained in greater detail in § 6.4.

6.3. Wall-normal or radial heat fluxes

A comparison of the inner and outer-normalised turbulent heat flux profiles is shown in Fig. 9. Existing (channel) and present (pipe) DNS data reveal that the traditional inner normalisation fails to

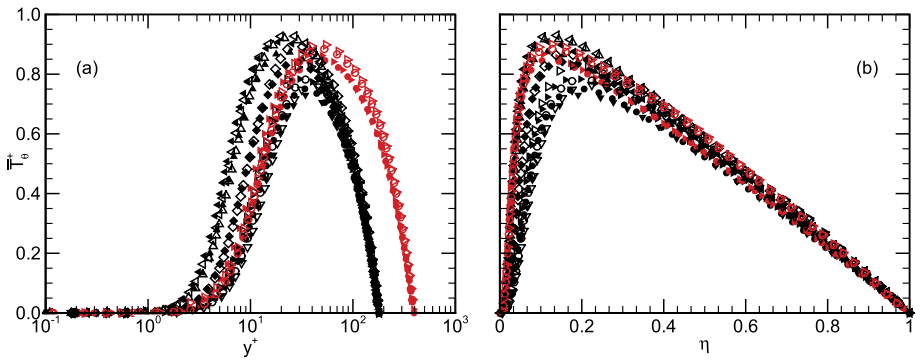

Fig. 9. Comparison of traditional (a) inner and (b) outer scaling of turbulent heat flux for pipe and channel. Symbol shapes for DNS data are given in Table 2. All black symbols represent data for $Re_\tau = 180$ and $0.6 \leq Pr \leq 7.0$, and red symbols for $Re_\tau = 395$ and $Pr = 0.71, 1.0$. (For interpretation of the references to colour in this figure legend, the reader is referred to the web version of this article.)

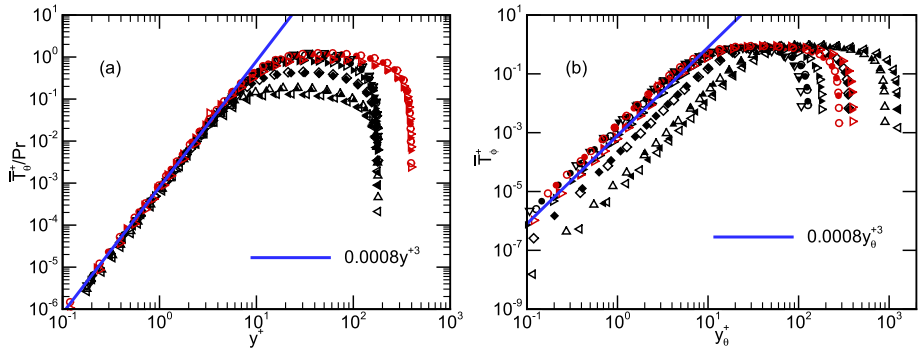

Fig. 10. Comparison of inner scaling of turbulent heat flux for pipe and channel. (a) Alternate inner scaling and (b) proposed inner scaling (30) for $b = 1$. Symbol shapes for DNS data are given in Table 2. All black symbols represent data for $Re_\tau = 180$ and $0.6 \leq Pr \leq 7.0$, and red symbols for $Re_\tau = 395$ and $Pr = 0.71, 1.0$. (For interpretation of the references to colour in this figure legend, the reader is referred to the web version of this article.)

yield an invariant profile for varying Reynolds and Prandtl numbers even within a couple of y^+ units from the wall. These profiles also display an apparent flow configuration influence. For $Pr > 0.71$, traditional outer normalization, however, yields a much tighter clustering of the profiles over an outer domain that extends from the centreline inward. Neither of these normalizations yields an invariant profile in the vicinity of the peak. It is also apparent from Fig. 9(a) that for fixed Re_τ the inner normalised maximum turbulent heat flux location moves outward with increasing Prandtl number, while the outer normalized peak location moves inward (Fig. 9(b)). Furthermore, the outer normalised pipe flow profile shows a noticeably higher value than for the channel flow. Piller [19] and Redjem-Saad et al. [21] also observed the similar behaviour of higher intensity temperature fluctuations for pipe flow when compared with channel flow.

Many researchers [14,21,24,38] have suggested the alternate inner scaling of turbulent heat flux based on a Taylor series expansion about the wall. In order to display the near wall effect, this alternate scaling modifies the turbulent heat flux normalised by Prandtl number as shown in Fig. 10(a). One of the interesting features of this scaling is that at comparable parameter values the pipe and channel flow profiles are convincingly the same. Unlike the mean temperature, our proposed inner normalization (30) using $b = 1$ does not produce an invariant heat flux profile. Fig. 10(b) shows that this normalization exhibits a strong dependence on both Reynolds and Prandtl numbers. This apparent limitation of the proposed scaling (30) was previously reported in Saha et al. [28]. For channel flow, the relevant observation here is that the mean temperature profile adjacent to the wall can be made invariant by stretching either $\overline{\Theta}^+$ or y^+ by a function of Pr. For the heat flux, however, invariance is only attained by self-consistently stretching $\overline{T}_\theta^+$.

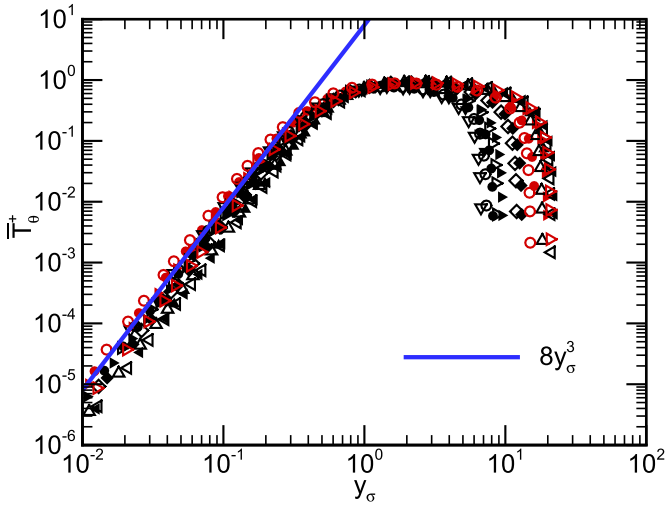

Fig. 11. Comparison of inner scaling of turbulent heat flux for pipe and channel following Wei et al. [25] as mentioned in (27). Symbol shapes for DNS data are given in Table 2. All black symbols represent data for $Re_\tau = 180$ and $0.6 \leq Pr \leq 7.0$, and red symbols for $Re_\tau = 395$ and $Pr = 0.71, 1.0$. (For interpretation of the references to colour in this figure legend, the reader is referred to the web version of this article.)

The scaling proposed by Wei et al. [25] as mentioned in (27) causes the profiles to approximately merge near the wall (see Fig. 11). Note also that the peak values of the profiles increase toward unity with increasing Reynolds and Prandtl numbers. The normalised heat flux profiles, however, indicate a noticeable dependence on the duct geometry from the near-wall region to the centre of the pipe (open symbols) or channel (closed symbols).

6.4. Streamwise heat fluxes

The streamwise turbulent heat flux, $\overline{T}_s^+ = \langle u_x' T' \rangle^+$, normalized by the friction velocity and temperature is shown in Fig. 12. The traditional inner and outer normalisations of the streamwise heat flux profiles do not distinguish in the respective inner and outer regions between the pipe and the channel results. These observations agree well with the comparisons performed by Piller [19] and Redjem-Saad et al. [21]. Upon closer inspection of these profiles, one notes a discrepancy in the peak values in these two flows. The value of $\overline{T}_s^+$ which increases with increasing Pr, has a slightly higher turbulent heat flux $\overline{T}_{s,\text{peak}}^+ = 18.69$ for pipe compared with channel flow $\overline{T}_{s,\text{peak}}^+ = 18.28$ at $Pr = 7$ and $Re_\tau = 180$. Moreover, the location of the near-wall peak flux seems to shift towards the wall with increasing Pr and Re_τ. Another observation is noticed in the outer core region. The outer-normalised heat flux profiles (Fig. 12(b)) exhibit an identical curve for both pipe and channel flows. This is interesting since the respective streamwise velocity [6] or temperature rms under outer normalisation each possess a slightly greater value for pipe DNS than for channel DNS.

An alternate inner scaling using the ratio of $\overline{T}_s^+/Pr$ is shown in Fig. 13(a) with emphasis on the near-wall region. Taylor series expansion of the temperature and velocity fluctuations allows the streamwise heat flux to be expressed as

$$\overline{T}_s^+ = Pr\left(\overline{b_x b_\theta} y^{+2} + \overline{c_x c_\theta} y^{+3} + \ldots\right), \tag{33}$$

where the correlation coefficient $\overline{b_x b_\theta}$ in the vicinity of the wall is expected to be independent of Pr within the selected range. Both

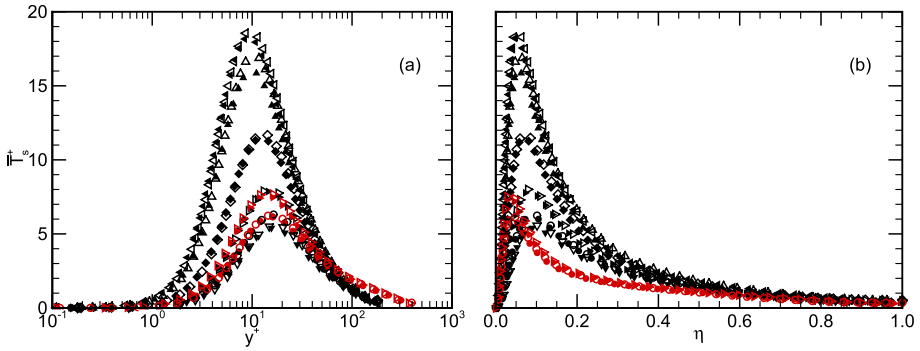

Fig. 12. Comparison of traditional (a) inner and (b) outer scaling of streamwise turbulent heat flux for pipe and channel. Symbol shapes for DNS data are given in Table 2. All black symbols represent data for $Re_\tau = 180$ and $0.6 \leq Pr \leq 7.0$, and red symbols for $Re_\tau = 395$ and $Pr = 0.71, 1.0$. (For interpretation of the references to colour in this figure legend, the reader is referred to the web version of this article.)

Kawamura et al. [24] and Redjem-Saad et al. [21] presented this alternate inner-normalization for channel and pipe flows, respectively. The near-wall behaviour is revealed for both channel and pipe flows in the present comparison. A weak dependence on Pr is evident in Fig. 13(a). Similar to $\overline{T}^+_\theta$, the proposed inner-scaled profiles fail to merge in the vicinity of the wall for varying Re_τ and Pr.

The reasons for higher amplitude thermal statistics in the pipe when compared to the channel remains an open question. Piller [19] and Redjem-Saad et al. [21] suggested the effect of wall curvature. The decreasing region of interaction from the opposing wall offers a separate explanation (see Fig. 14). Similar to the explanation proposed by Chin [6] for velocity statistics, pipe flow forces the motions near the centerline to interact more vigorously; possibly leading to higher velocity fluctuations. Similarly, the inward applied heat flux contributes more strongly to higher temperature fluctuations in pipe flows, whereas in the channel the distribution of applied heat flux in the spanwise direction has a weaker interaction in the core region.

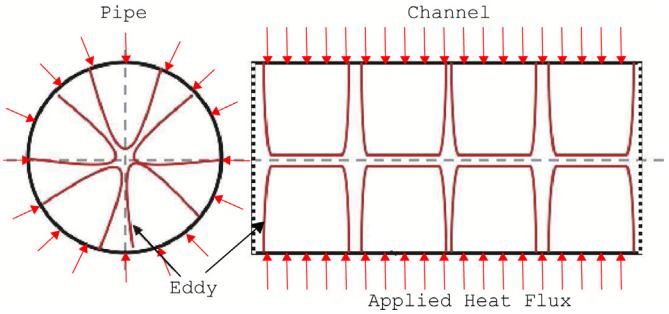

Fig. 14. Schematic of applied heat flux and eddies in pipe and channel cross-section, views taken along mean flow direction. This figure is adapted and modified from [6].

7. Comparisons of intermediate layer normalizations

From the analysis of the mean energy equation discussed at the outset, layer III is where all three of the terms in Equation (27) or (30) have the same order of magnitude. Regardless of Re_τ or Pr this occurs in a region surrounding the peak turbulent heat flux. Our goal is to rescale (27) or (30) such that all the terms are formally $O(1)$ in layer III. Following Wei et al. [25], a successful rescaling will take the form

$$\widehat{y_\sigma} = \sigma(y_\sigma - y_{\sigma m}),\ \widehat{T_\theta} = (1/\sigma)\left(\overline{T}^+_\theta - \overline{T}^+_{\theta m}\right),\ \widehat{\psi} = \psi - \psi_m, \tag{34}$$

where $y_{\sigma m}$ is the location of the peak turbulent heat flux, $\overline{T}^+_{\theta m}$ are the peak value of turbulent heat flux and ψ_m is the normalised mean temperature at $y_{\sigma m}$ (see Saha et al. [28]). Using the above variables, the invariant form of the mean energy Equation (27) becomes

$$\frac{d^2\widehat{\psi}}{d\widehat{y}^2_\sigma} + \frac{d\widehat{T_\theta}}{d\widehat{y}_\sigma} + 1 = 0. \tag{35}$$

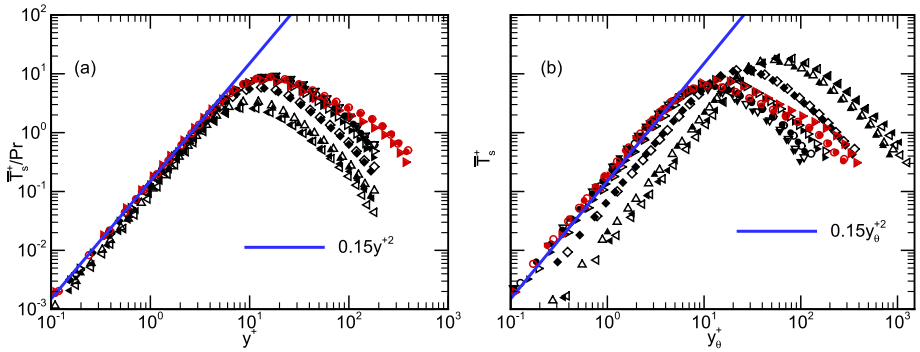

Fig. 13. Comparison of inner scaling of streamwise turbulent heat flux for pipe and channel. (a) Alternate inner scaling (33) and (b) proposed inner scaling (30) for $b = 1$. Symbol shapes for DNS data are given in Table 2. All black symbols represent data for $Re_\tau = 180$ and $0.6 \leq Pr \leq 7.0$, and red symbols for $Re_\tau = 395$ and $Pr = 0.71, 1.0$. (For interpretation of the references to colour in this figure legend, the reader is referred to the web version of this article.)

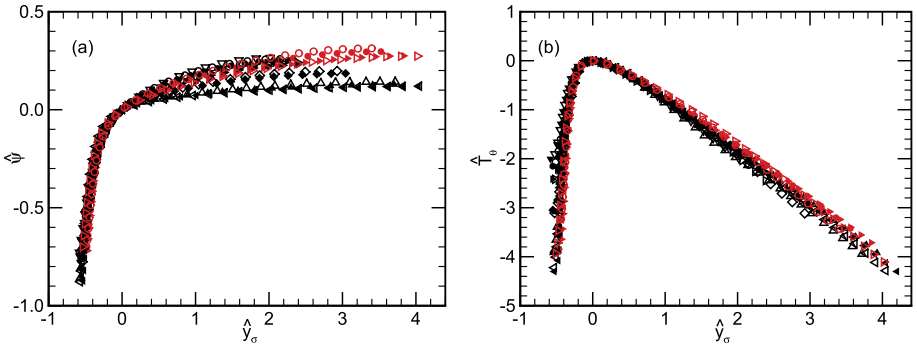

Fig. 15. Comparison of mesoscaling of (a) mean temperature and (b) turbulent heat flux between pipe and channel following Wei et al. [25] as mentioned in (35). Symbol shapes for DNS data are given in Table 2. All black symbols represent data for $Re_\tau = 180$ and $0.6 \leq Pr \leq 7.0$, and red symbols for $Re_\tau = 395$ and $Pr = 0.71, 1.0$. (For interpretation of the references to colour in this figure legend, the reader is referred to the web version of this article.)

The desired invariant form is attained, as all of the normalized terms are formally $O(1)$. Note that $\mathrm{d}\overline{T}_\theta^+/\mathrm{d}\eta$ is formally equal to $\mathrm{d}\widehat{T}_\theta/\mathrm{d}\widehat{y}_\sigma$, and thus the intermediate scaled Equation (35) identically matches the outer normalised Equation (26). This indicates that the intermediate scaling should be appropriate for the turbulent heat flux data into the outer region as long as the peak position is set at the origin.

As explained in Saha et al. [28], the above formulation (35) fails to produce invariant profiles of mean temperature in channel DNS. Hence, it is our natural interest to investigate the existence of invariant profiles for both pipe and channel using our proposed scaling. This is done by repeating the rescaling procedure just described to yield (35), but beginning with (36). Doing this reveals that the inner normalised form of the mean energy Equation (30) has corresponding intermediate variables

$$\widehat{y} = \sqrt{\frac{Pr}{\delta^+}}\left(y^+ - y_m^+\right) = \sqrt{\delta^+ Pr}(\eta - \eta_m), \tag{36}$$

$$\widehat{T}_\phi = \sqrt{\delta^+ Pr}\left(\overline{T}_\theta^+ - \overline{T}_{\theta m}^+\right), \tag{37}$$

$$\widehat{\Theta} = \left(\overline{\Theta}^+ - \overline{\Theta}_m^+\right). \tag{38}$$

Since the above meso-scaled variables do not depend on the coefficient b, it is expected to yield a universal form of (30), also see Seena and Afzal [39]. The resulting invariant form of the mean energy equation is

$$\frac{\mathrm{d}^2\widehat{\Theta}}{\mathrm{d}\widehat{y}^2} + \frac{\mathrm{d}\widehat{T}_\phi}{\mathrm{d}\widehat{y}} + 1 = 0. \tag{39}$$

We explore the profile behaviours implied by (35) and (39).

Fig. 15 shows the profile normalizations of the mean temperature and turbulent heat flux associated with (35). As indicated, this formulation fails to produce invariant mean temperature profiles from $\widehat{y}_{\sigma m}$ to the outer region. On the other hand, the heat flux profiles under this normalization appear to merge, at least approximately. As previously shown for channel flow [28], these behaviours stem from introducing a normalized temperature function other than Θ^+. Interestingly, while the mean temperature profiles are not invariant, there do not appear to be any significant differences in the meso-scaled profiles from the pipe and channel. This reinforces the intermediate scaling strategy explored by Wei et al. [4] for the Reynolds shear stress.

Fig. 16 shows the mean temperature and heat flux scaled according to (39). Over the relevant domain, all of the profiles merge onto a single curve under the coordinate stretching produced by the variables $\widehat{y}$, $\widehat{\Theta}$ and $\widehat{T}_\phi$. This scaling for mean temperature and turbulent heat flux is apparently valid over an interior region that extends from inside the peak in $\overline{T}_\theta^+$ to a zone near the centerline. In general, the theory indicates that this scaling should be valid in a domain surrounding $y_m^+(\widehat{y} = 0, \widehat{T}_\phi = 0)$ having an extent of $\Delta\widehat{y} = O(1)$. As noted previously, however, this scaling naturally melds with outer scaling, and thus in these coordinates it is analytically predicted to extend to the centerline. Within the domain just described, no significant differences between pipe and channel flow data are observed (similar to the results of Wei et al. [4]). For the present data sets, this domain extends from

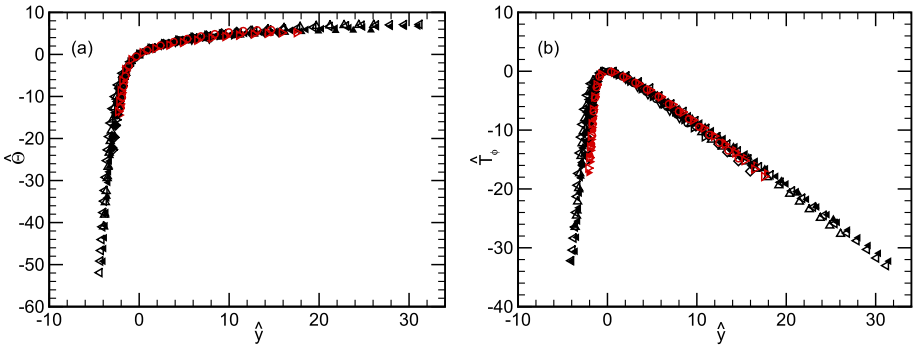

Fig. 16. Comparison of the proposed mesoscaling (39) of (a) mean temperature and (b) turbulent heat flux between pipe and channel. Symbol shapes for DNS data are given in Table 2. All black symbols represent data for $Re_\tau = 180$ and $0.6 \leq Pr \leq 7.0$, and red symbols for $Re_\tau = 395$ and $Pr = 0.71, 1.0$. (For interpretation of the references to colour in this figure legend, the reader is referred to the web version of this article.)

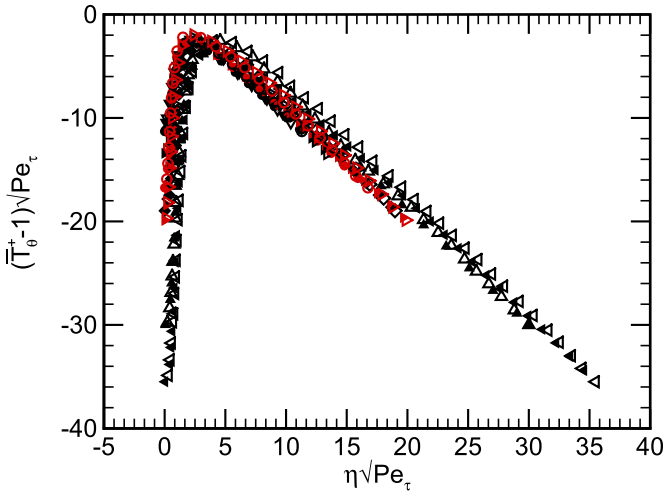

Fig. 17. Comparison of approximate mesoscaling (41) of turbulent heat flux between pipe and channel. Symbol shapes for DNS data are given in Table 2. All black symbols represent data for $Re_\tau = 180$ and $0.6 \le Pr \le 7.0$, and red symbols for $Re_\tau = 395$ and $Pr = 0.71, 1.0$. (For interpretation of the references to colour in this figure legend, the reader is referred to the web version of this article.)

$-2 < \widehat{y} < 32$. The intermediate scaling does not, however, hold in a narrow region near the wall. This is where the scaling patch associated with inner length is expected to hold. Like the mean temperature profile, the scaled turbulent heat flux profiles convincingly support the theory, as the profiles of Fig. 16(b) increasingly merge onto a single curve with increasing Peclet number ($Pe_\tau = \delta^+ Pr$). The lack of a proper inner scaled thermal heat flux indirectly restricts the generality of this approach all the way to the wall. This is further demonstrated by considering the properties of the underlying layer hierarchy (explained below).

In order to evaluate the mesoscaled variables $\widehat{y}$ and $\widehat{T}_\phi$, one requires prior knowledge of the maximum turbulent heat flux value and its location. Due to the limitation of precisely determining the value of η_m and $\overline{T}^+_{\theta m}$, Wei et al. [4] proposed an 'approximate' mesoscaling. This scaling is based upon the limiting behaviours of η_m and $\overline{T}^+_{\theta m}$, which can be estimated for sufficiently high Peclet number ($Pe_\tau = \delta^+ Pr$) as follows

$$\eta_m = O\left(1/\sqrt{Pe_\tau}\right), \overline{T}^+_{\theta m} = 1 - O\left(1/\sqrt{Pe_\tau}\right). \tag{40}$$

From this, (36) and (37) then yield

$$\widehat{y} = \sqrt{Pe_\tau}\eta - O(1), \widehat{T}_\phi = \sqrt{Pe_\tau}\left(\overline{T}^+_\theta - 1\right) + O(1). \tag{41}$$

Thus an approximate scaling (41) can be constructed by plotting $\sqrt{Pe_\tau}(\overline{T}^+_\theta - 1)$ versus $\sqrt{Pe_\tau}\eta$, without necessarily knowing the value of η_m and $\overline{T}^+_{\theta m}$. As shown in Fig. 17, the turbulent heat flux profiles for both pipe and channel flows nominally merge to a single curve, particularly for the higher Peclet number. This approximate scaling is theoretically expected to improve with increasing Peclet number.

8. Length scale hierarchy for the thermal field

The balance breaking and exchange of terms in layer III (as shown in Fig. 2) is a consequence of a continuum of scaling layers. This approach is analogous to the scaling behaviours for the momentum field as first introduced by Fife et al. [40]. Using the invariant form of the mean energy equation, Wei et al. [25] revealed a self-similar structure, where the heat transfer occurs across a hierarchy of layers, each of which having a distinct characteristic width. In the present study, deeper consideration of (35) or (39) reveals that the associated intermediate normalization arises as an average property of an underlying continuous hierarchy of scaling layers [25,28]. We denote this as the $L_\in$ layer hierarchy. This hierarchy is bounded in space between the positive and negative peaks in dT_θ/dy. Importantly, across each layer on the hierarchy there is a balance breaking and exchange of terms, in (35) or (39), that occurs at increasing scale with distance from the wall.

The self-similar heat transfer mechanism from layer to layer can be revealed from the invariant form of the mean energy Equation (35) or (39). A primary characteristic of the $L_\in$ hierarchy is its associated length distribution, W, which measures the width of each $L_\in$ layer as a function of y_σ or y^+_θ. Here L denotes any given layer on the hierarchy and the subscript to its dependence on the parameter $\in$ given by (43). The width of these scaling layers increases with distance from very near the wall to near the pipe or channel centreline. Analogous to the momentum analysis, from the decay rate of the turbulent heat flux gradient, it is possible to calculate the layer width distribution, W across the hierarchy. Wei et al. [25] show that

$$W(y_\sigma) = O\left(\in^{-1/2}\right), \tag{42}$$

where the parameter $\in$ is expressed as

$$\in = \frac{d\overline{T}^+_\theta}{dy_\sigma} + \sigma^2 R_\sigma(y_\sigma). \tag{43}$$

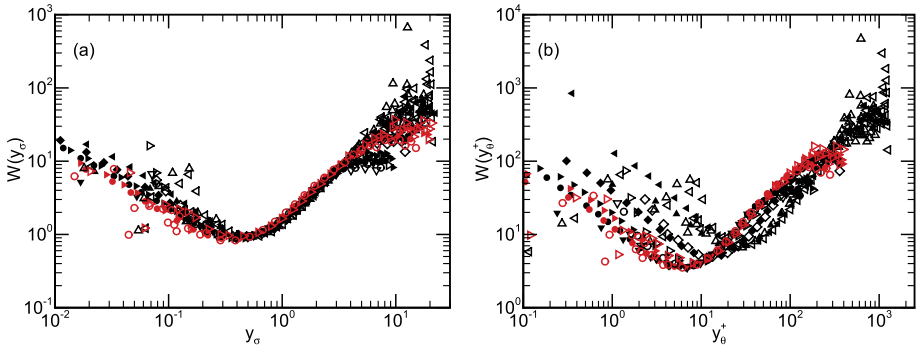

Fig. 18. Comparison of layer width distribution of the $L_\in$ hierarchy for heat transfer in pipe and channel flow. (a) Formulation based on Wei et al. [25] as mentioned in (42) and (b) present case for $b = 1$. Symbol shapes for DNS data are given in Table 2. All black symbols represent data for $Re_\tau = 180$ and $0.6 \le Pr \le 7.0$, and red symbols for $Re_\tau = 395$ and $Pr = 0.71, 1.0$. (For interpretation of the references to colour in this figure legend, the reader is referred to the web version of this article.)

We are able to evaluate the criterion for the logarithmic-like dependence of the normalised mean temperature with increasing Reynolds and Prandtl numbers. A linear $W(y_\sigma)$ profile (exact or approximate) is formally required for there to exist an exact or approximately logarithmic mean temperature profile [25]. Fig. 18 shows the comparison of the $W(y_\sigma)$ and similarly $W(y_\theta^+)$ profiles for the channel and pipe flows of Table 2. Scaled mean temperature profile data (Fig. 18(a)) suggest that logarithmic-like dependence begins to emerge for $y_\sigma \geq 1$. Indications from the momentum field analysis indicate, however, that the inertial log layer occurs beyond the peak in the Reynolds stress. Thus, the expectation here is that the "true" log layer for temperature occurs beyond the peak in $\overline{T}_\theta^+$, see Fig. 11. Comparisons reveal, however, that the logarithmic mean temperature profile is more subtly established than for the mean velocity profile [41]. One of the remarkable observations is that the W distribution is almost invariant over the interior domain of interest for the formulation of Wei et al. [25], whereas the formulation underlying the invariant form (39) shows sharp distinction between the $W(y_\theta^+)$ profiles at different Re_τ and Pr. From Fig. 18 it is also clear that higher Re_τ data (at any fixed Pr) are needed to fully clarify the emergence of a logarithmic mean temperature profile.

9. Conclusion

DNS data for fully-developed turbulent pipe and channel flows have been utilized to explore the scaling properties of the mean thermal energy equation. The analysis employs a theory based on the magnitude ordering of terms in the mean equation. Identifying the leading order terms in the mean energy equation of turbulent pipe flow reveals a four layer structure. This structure depends on Re_τ and Pr, and is similar to that found for channel flow. The traditional inner scale is transformed into a new inner length, and the invariant form admitted by the relevant form of the mean energy equation is determined. These invariant forms apply to inner, outer and intermediate regions of the flow, whose properties are dependent on a small parameter that is a function of Reynolds and Prandtl numbers. The present methodology scaled the turbulent heat flux, and the mean temperature over a considerable domain centred about the peak heat flux location. The present framework is analogous to that used for the Reynolds shear stress by Wei et al. [4], and also verifies their earlier findings for the intermediate layer scaling [25]. The existence and properties of the $L_\in$ layer hierarchy has been revealed in the simulation data, although it is also clear that higher Re_τ data are needed to more fully assess the scalings derived.

We conclude the following. The mean energy equation normalised under inner and outer scaling reveals the same form except the mean streamwise advection that depends on the flow geometry. Similarly, the onset of the four layer thermal regime occurs when $Pr \geq 0.6$ for $Re_\tau \geq 180$. The mean temperature profiles under traditional inner normalisation show agreement between the two flows, except in the core region. On the other hand, the proposed inner scaling yields invariant mean temperature profiles independent of duct wall curvature. The proposed inner scaling for turbulent heat flux, however, fails to yield an invariant curve, and shows strong variation between pipe and channel flows. The proposed intermediate layer scaling approach successfully scales both mean temperature and turbulent heat flux independent of any flow configurations and conditions except very close to the wall. Moreover, the turbulent heat flux data accepts the applicability of 'approximate' meso-scaling valid for both pipe and channel flows. The profile of the layer hierarchy associated with the intermediate normalization is not invariant under the proposed normalisation. However, the existing scaling theory by Wei et al. [25] produces an approximately invariant layer width distribution.

Acknowledgements

The authors gratefully acknowledge the financial support of the Australian Research Council (Grant No. DP120101467 and LP120100233) and the computational resources provided by a Victorian Life Sciences Computation Initiative (VLSCI) grant number VR0210 on its Peak Computing Facility at the University of Melbourne, an initiative of the Victorian Government, Australia.

Nomenclature

Greek symbols

α	thermal diffusivity of fluid
β	additive constant for temperature
Δ	difference operator
δ	half channel height or pipe radius
δ^+	Reynolds number based on friction velocity or Kármán number
η	wall normal distance normalized by half channel height or pipe radius
η_m	outer scaled location of maximum turbulent heat flux
Γ	exponential parameter defined in (3)
$\in$	small positive number
κ_θ	von Kármán constant for temperature
∇	gradient operator
∇^2	Laplacian operator
ν	kinematic viscosity of fluid
ϕ	small parameter
π	mathematical constant (≈ 3.14159)
ψ	normalized mean temperature
ψ_m	normalized mean temperature at $y_{\sigma m}$
ρ	mass density of fluid
σ	small parameter
Θ	(dimensionless) temperature normalized by reference temperature
θ	azimuthal distance
ε	small parameter
Θ_c	(dimensionless) temperature at the pipe centre
Θ_m	(dimensionless) temperature at y_m

Other symbols

$(\,)'$	fluctuating component
$(\,)^+$	scaling with friction velocity
$\overline{(\,)}$	spatial averaging
$\widehat{(\,)}$	rescaled function
$\langle\,\rangle$	spatial and temporal averaging
$\lvert\,\rvert$	absolute value

Roman symbols

$\mathbf{F}$	driving force vector
$\mathbf{U}$	(dimensionless) velocity vector normalized by bulk velocity
$\mathbf{u}$	velocity vector
A	gradient of the molecular diffusion flux
B	gradient of the turbulent transport flux
b	a constant coefficient
b_θ	coefficient of Taylor's series expansion
b_x	coefficient of Taylor's series expansion
C	mean streamwise advection
c_θ	coefficient of Taylor's series expansion
C_p	specific heat at constant pressure
c_x	coefficient of Taylor's series expansion
D	pipe diameter

F_x axial force per unit mass for smooth wall pipe
k_c thermal conductivity of fluid
L computational or domain length in streamwise direction
$L_\in$ scaling layer
N non-linear terms in the Navier–Stokes or energy equation
P kinematic pressure
p pressure
P_b (dimensionless) kinematic pressure normalized by bulk velocity
Pe_τ friction Peclet number
Pr Prandtl number
Q volumetric flow rate
q_w constant wall heat flux
r radial direction
R_σ scaled advection function
R_θ scaled advection function
R_s scaled advection function
Re_τ Reynolds number based on friction velocity or Kármán number
Re_D Reynolds number based on bulk velocity
T temperature
t time
T_τ friction temperature based on friction velocity
t_τ (dimensionless) time normalized by friction velocity and pipe diameter
T_b bulk temperature
t_b (dimensionless) time normalized by bulk velocity and pipe diameter
T_r reference temperature based on bulk velocity
T_w wall temperature
u_τ friction velocity
u_θ velocity in azimuthal direction
u_b bulk velocity
u_r velocity in radial direction
U_x (dimensionless) velocity normalized by bulk velocity in streamwise direction
u_x velocity in streamwise direction
W width of layer hierarchy
X (dimensionless) distance normalized by pipe diameter in streamwise direction
x streamwise distance
y wall normal distance
y_σ inner scaled variable
y_θ^+ inner scaled variable depends on Prandtl number and friction velocity
y_m wall normal location of maximum turbulent heat flux
$y_{\sigma m}$ inner scaled location of maximum turbulent heat flux
z spanwise distance (reference to channel flow only)
T_ϕ modified radial (pipe) or wall-normal (channel) turbulent heat flux
T_θ radial (pipe) or wall-normal (channel) turbulent heat flux
T_s streamwise turbulent heat flux
$T_{\theta m}$ maximum radial (pipe) or wall-normal (channel) turbulent heat flux

References

[1] P. Monty, A. Stewart, C. Williams, S. Chong, Large-scale features in turbulent pipe and channel flows, J. Fluid Mech. 589 (2007) 147–156.
[2] P. Monty, N. Hutchins, C.H. Ng, I. Marusic, S. Chong, A comparison of turbulent pipe, channel and boundary layer flows, J. Fluid Mech. 632 (2009) 431–442.
[3] T. Wei, P. Fife, J.C. Klewicki, P. McMurtry, Properties of the mean momentum balance in turbulent boundary layer, pipe and channel flows, J. Fluid Mech. 522 (2005) 303–327.
[4] T. Wei, P. McMurtry, J.C. Klewicki, P. Fife, Mesoscaling of Reynolds shear stress in turbulent channel and pipe flows, AIAA J. 43 (11) (2005) 2350–2353.
[5] H.C.H. Ng, J.P. Monty, N. Hutchins, M.S. Chong, I. Marusic, Comparison of turbulent channel and pipe flows with varying Reynolds number, Exp. Fluids 51 (2011) 1261–1281.
[6] C. Chin, Numerical Study of Internal Wall-bounded Turbulent Flows (Ph.D. thesis), Department of Mechanical Engineering, Univeristy of Melbourne, 2011.
[7] J.C. Klewicki, C. Chin, H.M. Blackburn, A. Ooi, I. Marusic, Emergence of the four layer dynamical regime in turbulent pipe flow, Phys. Fluids 24 (2012) 045107.
[8] J.C. Klewicki, Self-similar mean dynamics in turbulent wall flows, J. Fluid Mech. 718 (2013) 596–621.
[9] J. Elsnab, J.C. Klewicki, D. Maynes, T. Ameel, Mean dynamics of transitional channel flow, J. Fluid Mech. 678 (2011) 451–481.
[10] R.A. Gowen, J.W. Smith, The effect of the Prandtl number on temperature profiles for heat transfer in turbulent pipe flow, Chem. Eng. Sci. 22 (12) (1967) 1701–1711.
[11] B.A. Kader, Temperature and concentration profiles in fully turbulent boundary layers, Int. J. Heat Mass Transfer 24 (1981) 1541–1544.
[12] N. Kasagi, T. Tomita, K. Kuroda, Direct numerical simulation of passive scalar field in a turbulent channel flow, J. Heat Transfer 114 (3) (1992) 598606.
[13] A. Johansson, P.M. Wikström, DNS and modelling of passive scalar transport in turbulent channel flow with a focus on scalar dissipation rate modelling, Flow Turbul. Combust. 63 (1999) 223–245.
[14] H. Kawamura, H. Abe, Y. Matsuo, DNS of turbulent heat transfer in channel flow with respect to Reynolds and Prandtl number effects, Int. J. Heat Fluid Flow 20 (1999) 196–207.
[15] H. Kawamura, H. Abe, K. Shingai, DNS of turbulence and heat transport in a channel flow with different Reynolds and Prandtl numbers and boundary conditions, in: Y. Nagano, K. Hanjalic (Eds.), 3rd International Symposium on Turbulence, Heat and Mass Transfer, April 3–6 2000, pp. 15–32. Nagoya, Japan.
[16] H. Kawamura, H. Abe, DNS of turbulent scalar transport in a channel flow up to $Re_\tau = 640$ with $Pr = 0.025$ and 0.71, in: Seventh TRA Conference, Seoul Nat'l Univ., Seoul, Korea, 27 April 2002, pp. 65–79.
[17] P. Orlandi, S. Leonardi, Passive scalar in a turbulent channel flow with wall velocity disturbances, Flow Turbul. Combust. 72 (2004) 181–197.
[18] H. Abe, H. Kawamura, Y. Matsuo, Surface heat-flux fluctuations in a turbulent channel flow up to $Re_\tau = 1020$ with $Pr = 0.025$ and 0.71, Int. J. Heat Fluid Flow 25 (3) (2004) 404–419.
[19] M. Piller, Direct numerical simulation of turbulent forced convection in a pipe, Int. J. Numer. Methods Fluids 49 (2005) 583–602.
[20] S. Satake, T. Kunugi, R. Himeno, High Reynolds number computation for turbulent heat transfer in a pipe flow, in: High Performance Computing, Third International Symposium, 2000, pp. 514–523. Tokyo, Japan.
[21] L. Redjem-Saad, M. Ould-Rouiss, G. Lauriat, Direct numerical simulation of turbulent heat transfer in pipe flows: effect of Prandtl number, Int. J. Heat Fluid Flow 28 (5) (2007) 847–861.
[22] W.K. George, Is there a universal log law for turbulent wall-bounded flows? Philos. Trans. R. Soc. A 365 (2007) 789–806.
[23] M. Kozuka, Y. Seki, H. Kawamura, DNS of turbulent heat transfer in a channel flow with a high spatial resolution, Int. J. Heat Fluid Flow 30 (3) (2009) 514–524.
[24] H. Kawamura, K. Ohsaka, H. Abe, K. Yamamoto, DNS of turbulent heat transfer in channel flow with low to medium-high Prandtl number fluid, Int. J. Heat Fluid Flow 19 (5) (1998) 482–491.
[25] T. Wei, P. Fife, J.C. Klewicki, P. McMurtry, Scaling heat transfer in fully developed turbulent channel flow, Int. J. Heat Mass Transfer 48 (2005) 5284–5296.
[26] A. Seena, A. Bushra, N. Afzal, Logarithmic expansions for Reynolds shear stress and Reynolds heat flux in a turbulent channel flow, J. Heat Transfer 130 (9) (2008) 094501.
[27] A. Seena, N. Afzal, Power law velocity and temperature profiles in a fully developed turbulent channel flow, J. Heat Transfer 130 (9) (2008) 091701.
[28] S. Saha, J.C. Klewicki, A.S.H. Ooi, H.M. Blackburn, T. Wei, Scaling properties of the equation for passive scalar transport in wall-bounded turbulent flows, Int. J. Heat Mass Transfer 70 (2014) 779–792.
[29] H. Blasius, Das Ähnlichkeitsgesetz bei Reibungsvorgängen in Flüssigkeiten, in: Mitteilungen ber Forschungsarbeiten auf dem Gebiete des Ingenieurwesens, vol. 131, Springer, Berlin Heidelberg, 1913, pp. 1–41.
[30] D.M. McIver, H.M. Blackburn, G.J. Nathan, Spectral element – Fourier methods applied to simulation of turbulent pipe flow, ANZIAM J. 42 (E) (2000) C954–C977.
[31] C. Chin, A.S.H. Ooi, I. Marusic, H.M. Blackburn, The influence of pipe length on turbulence statistics computed from direct numerical simulation data, Phys. Fluids 22 (2010) 115107.
[32] C. Chin, A.S.H. Ooi, I. Marusic, H.M. Blackburn, The influence of pipe length in direct numerical simulation, in: 17th Australasian Fluid Mechanics Conference, Auckland, New Zealand, 5–9 December 2010.
[33] S. Saha, C. Chin, H.M. Blackburn, A.S.H. Ooi, The influence of pipe length on thermal statistics computed from DNS of turbulent heat transfer, Int. J. Heat Fluid Flow 32 (6) (2011) 1083–1097.
[34] H.M. Blackburn, S.J. Sherwin, Formulation of a Galerkin spectral element–Fourier method for three-dimensional incompressible flows in cylindrical geometries, J. Comput. Phys. 197 (2) (2004) 759–778.
[35] S. Saha, Numerical Analysis of Turbulent Heat Transfer in Pipe and Channel Flows (Ph.D. thesis), Department of Mechanical Engineering, Univeristy of Melbourne, 2014.

[36] Y. Seki, H. Kawamura, DNS of turbulent heat transfer in a channel flow with a varying streamwisely thermal boundary condition, Heat Transfer Asian Res. 35 (4) (2006) 265–278.
[37] H. Abe, H. Kawamura, Y. Matsuo, DNS of turbulent heat transfer in channel flow: near-wall turbulence quantities, in: 13th Australasian Fluid Mechanics Conference, 13–18 December 1998, pp. 849–852. Melbourne, Australia.
[38] H. Kawamura, K. Ohsaka, K. Yamamoto, DNS of turbulent heat transfer in channel flow with low to medium-high Prandtl number fluid, in: 11th Symposium Turbulent Shear Flows, vol. 1, 8-11 September 1997, pp. 8.7–8.12. Grenoble, France.
[39] A. Seena, N. Afzal, Intermediate scaling of turbulent momentum and heat transfer in a transitional rough channel, J. Heat Transfer 130 (2008) 031701.
[40] P. Fife, J. Klewicki, P. McMurtry, T. Wei, Multiscaling in the presence of indeterminacy: wall-induced turbulence, Multiscale Model. Simul. 4 (3) (2005) 936–959.
[41] J.C. Klewicki, P. Fife, T. Wei, On the logarithmic mean profile, J. Fluid Mech. 638 (2009) 73–93.